Deep-water coral records of glacial and recent ocean-atmosphere dynamics from the Perth Canyon in the southeast Indian Ocean

Julie A Trotter, Malcolm T Mcculloch, Juan Pablo d'Olivo, Pete Scott, Nadine Tisnérat-Laborde, Marco Taviani, Paolo Montagna

Quaternary Science Advances 6 (2022) 100052

Contents lists available at ScienceDirect

Quaternary Science Advances

journal homepage: www.sciencedirect.com/journal/quaternary-science-advances

Deep-water coral records of glacial and recent ocean-atmosphere dynamics from the Perth Canyon in the southeast Indian Ocean

Julie A. Trotter [a,*], Malcolm T. McCulloch [a], Juan Pablo D'Olivo [a], Pete Scott [a], Nadine Tisnérat-Laborde [b], Marco Taviani [c,d], Paolo Montagna [e]

[a] Oceans Graduate School and UWA Oceans Institute, The University of Western Australia, 35 Stirling Highway Perth, 6009, Western Australia, Australia
[b] LSCE/IPSL, Laboratoire des Sciences du Climat et de l'Environnement, Av. de la Terrasse, 91198, Gif-sur-Yvette, France
[c] Istituto di Scienze Marine (ISMAR), Consiglio Nazionale delle Ricerche (CNR), Via Gobetti 101, Bologna, Italy
[d] Stazione Zoologica Anton Dohrn, Villa Comunale, 80121, Napoli, Italy
[e] Istituto di Scienze Polari (ISP), Consiglio Nazionale delle Ricerche (CNR), Via Gobetti 101, Bologna, Italy

ARTICLE INFO

Keywords:
Deep-water coral
Indian Ocean
Nd isotopes
Ocean ventilation
Last Glacial Maximum
Perth Canyon

ABSTRACT

We present radiocarbon and neodymium isotope records from accurately dated (U-series) live and fossil (<2 ka, 17.5 to 29.6 ka BP) deep-water corals, collected between 675 and 1788 m from the Perth Canyon, offshore southwest Australia. These records provide the first insights into recent and last glacial intermediate-deep water circulation and ventilation histories from the poorly represented southeast Indian Ocean. Ocean ventilation fluctuated significantly during the last glacial period, being highly ventilated during early Marine Isotope Stage 2 and the early deglaciation, yet less ventilated and more stratified during the Last Glacial Maximum. Furthermore, the Perth Canyon corals recorded a major and rapid (~300 years) perturbation at 25 ka, indicating that mid-depth waters were exposed to poorly ventilated, unradiogenic Nd deeper waters. We link this to similar, age equivalent changes at geographically disparate sites from the southeast Atlantic to the Southern Ocean south of Tasmania, together with fluctuations in Antarctic sea-ice, oceanic fronts, and Atlantic Meridional Overturning Circulation (AMOC). This widespread Southern Ocean event indicates a transient breach in upper and lower ocean cell boundaries of the MOC, providing further evidence for the non-steady state, zonal dynamics of the glacial Southern Ocean.

1. Introduction

The Southern Ocean is a key controller of the ocean-climate system and global carbon cycle, playing a major role in the exchange, storage, and redistribution of heat, CO_2, and nutrients throughout the oceans (e.g. Sarmiento et al., 2004). This is mainly a result of its unique position, with the World's largest ocean current, the intense westerly wind-driven Antarctic Circumpolar Current (ACC), flowing largely uninterrupted around the Antarctic continent. Apart from the Drake passage, the eastward flowing ACC is steered by local topography and is a significant influence on the globally important meridional overturning circulation (MOC) (Rintoul, 2018). South of the Polar Front, nutrient-rich and oxygen-depleted deep waters upwell and become ventilated as CO_2 is exchanged between the ocean and atmosphere. In this southern branch of the MOC near the Antarctic shelf, dense Antarctic Bottom Water is formed by cooling and brine formation, which sinks to become the dominant water mass of the abyssal oceans. In response to strong westerlies, the northwards flowing upper branch of the MOC becomes entrained into the Antarctic Intermediate Waters and overlying Sub-Antarctic Mode Waters (Rintoul, 2018). These northward flowing waters are responsible for nearly three-quarters of global marine biological production (Moore et al., 2018), and are the main source waters of the mid-latitude submarine canyons off southwest Australia (Woo and Pattiaratchi, 2008; Trotter et al., 2019), the area of our study site.

Considerable effort has focused on understanding these processes and the close inter-relationship between MOC and ACC, together with mechanisms driving major regime shifts in the oceans and consequent ocean-atmosphere interactions during glacial-interglacial cycles (e.g. Anderson et al., 2009; Sigman et al., 2010). The interdependencies between the location of sea-ice, oceanic fronts, westerly winds and changes in the strength of the ACC (Meredith, 2016), all modulate the carbon and associated nutrient inventories of the MOC (Laufkötter et al., 2016;

* Corresponding author.
E-mail address: julie.trotter@uwa.edu.au (J.A. Trotter).

https://doi.org/10.1016/j.qsa.2022.100052
Received 5 December 2021; Received in revised form 28 March 2022; Accepted 13 April 2022
Available online 16 April 2022

Marinov et al., 2006; Moore et al., 2018), as well as atmospheric CO_2 concentrations via ocean-atmosphere exchange (Marcott et al., 2014). Such changes in the Southern Ocean especially, are now recognised as the likely cause of lower atmospheric CO_2 concentrations during ice ages due to significant yet unconstrained changes in the carbon reservoir (Toggweiler and Russell, 2008; Sigman et al., 2010; Skinner et al., 2010). Likewise, there remains an incomplete understanding of the factors controlling ACC strength and hence possible abrupt mode changes in MOC. Such processes have major ramifications for our present-day climate regime as Antarctic ice-sheets again resume rapid large scale-melting with potential destabilisation of the ocean system (Rintoul et al., 2018). Thus, oceanographic and palaeo-seawater proxy studies of these water masses are important for deconvolving the complex interplay between ocean dynamics, seawater chemistry, and climate change, which can have global implications over both modern and longer timescales.

Changes in ocean-atmosphere dynamics and circulation patterns can be tracked using chemical tracers such as radiocarbon (^{14}C) (Broecker et al., 1984) and neodymium (Nd) isotopes (Piepgras and Wasserburg, 1980; Frank, 2002; Goldstein and Hemming, 2003). As atmospheric radiocarbon becomes sequestered by surface waters and transported into the deep ocean, the abundance of ^{14}C can be used to constrain the ages and ventilation histories of different water masses (e.g. Adkins and Boyle, 1997; Key, 2001; Matsumoto, 2007). Nd isotope compositions ($^{143}Nd/^{144}Nd$ ratios), conventionally expressed in ε_{Nd} notation (DePaolo and Wasserburg, 1976), can reveal the provenance and mixing of water masses that carry basin-specific fingerprints (e.g. Piepgras and Wasserburg, 1980; Frank, 2002; van de Flierdt et al., 2016; Tachikawa et al., 2017). Below ~500 m, waters from the Atlantic Ocean are characterised by low (unradiogenic) ε_{Nd} values (generally between −13 and −9) from old continental crust inputs, whereas higher values of the Pacific (−4 to −8) reflect the additional input of generally positive (radiogenic) ε_{Nd} from young volcanic island arcs, with the Southern and Indian Oceans having intermediate compositions (e.g. Piepgras and Wasserburg, 1980; McCulloch and Perfit, 1981; Bertram and Elderfield, 1993; Jeandel, 1993; Lacan et al., 2012; van de Flierdt et al., 2016; Tachikawa et al., 2017 and references therein; Lambelet et al., 2018; Amakawa et al., 2019).

Collectively, these highly complementary tracers can be used to characterise past ocean circulation patterns and shifts in carbon storage, which are central to understand the ocean-atmosphere-climate system. To constrain these processes and changes on timescales beyond modern seawater measurements, ^{14}C, $^{143}Nd/^{144}Nd$, together with radiometric dating (U/Th) have been applied to marine biogenic archives, such as deep-water corals and foraminifers (e.g. Adkins et al., 1998; Burton and Vance, 2000; Broecker et al., 2004; Piotrowski et al., 2004; Robinson et al., 2005; Pahnke et al., 2008; Mangini et al., 2010; Skinner et al., 2010; Burke and Robinson, 2012; Robinson et al., 2014; López Correa et al., 2012; Hu et al., 2016; Dubois-Dauphin et al., 2017; Basak et al., 2018; Wilson et al., 2020). Deep-water scleractinian corals have the advantage of being highly suitable for coupled ^{14}C and U/Th analyses, the latter due to the high uranium content in their aragonite skeletons which provides robust chronologies for palaeoseawater reconstructions. Their aragonite skeletons also directly record ambient seawater $^{143}Nd/^{144}Nd$ ratios (Copard et al., 2010; van de Flierdt et al., 2010) so the source of Nd is unequivocal.

Corals have been widely used to trace changes in ocean-atmosphere carbon exchange during periods of rapid climate change but historically focused on intermediate and deep waters of the Atlantic Ocean (e.g. Adkins et al., 1998; Robinson et al., 2005; Mangini et al., 2010), the Pacific (van de Flierdt et al., 2010), and most recently within the Southern Ocean around the Drake Passage (e.g. Robinson and van de Flierdt, 2009; Burke and Robinson, 2012; Wilson et al., 2020) and Tasmania (Hines et al., 2015). Conversely, coral ε_{Nd} records are few, and represent sites from the Atlantic Ocean and Drake Passage. Those fossil records generally support a stratified circulation model with significant shifts in North Atlantic Deep Water entering the Southern Ocean during major climate events in the last glacial-deglacial period (Robinson and van de Flierdt, 2009; Copard et al., 2010; Wilson et al., 2014, 2020; Struve et al., 2020). Very few coral records exist for the Indian Ocean, and none combining both ^{14}C and $^{143}Nd/^{144}Nd$, which is the focus of this study.

The Indian Ocean is the least studied of the major ocean basins, with the southern region having very limited coverage of seawater and geochemical palaeoproxy data. Prior Nd isotope proxy studies tracing Indian Ocean mid to deep water hydrodynamics are limited to glacial-interglacial foraminifer and sediment core records from the north, southwest, and south-central sectors. These studies have determined Antarctic Intermediate Water (AAIW) and Circumpolar Deep Water (CDW) recirculation pathways near Madagascar (Pahnke et al., 2008; Wilson et al., 2012; these sites mostly influenced by regional boundary exchange with volcanic sediments), the Bay of Bengal (Yu et al., 2018), changes in Atlantic-sourced deep water in the north central Indian Ocean (Piotrowski et al., 2009; Wilson et al., 2015), and long-term variability within Lower Circumpolar Deep Water (LCDW) around the Kerguelen Islands (Williams et al., 2021). Complementary foraminifer radiocarbon records have provided ventilation histories of CDW near Kerguelen, revealing that the southern Indian Ocean had a greater influence on atmospheric CO_2 and global carbon cycling during the last deglaciation than previously recognised (Gottschalk et al., 2020; Ronge et al., 2020). Palaeoclimate studies of subtropical southeast Indian Ocean and Southern Ocean foraminifers, offshore Western and South Australia, have inferred changes in ocean hydrography and climate from species abundances and $\delta^{18}O$ compositions over glacial-deglacial intervals (De Deckker et al., 2012, 2020).

Here we present the first deep-water coral environmental records from the Indian Ocean, which represent the only biogeochemical data from mid to deep waters of the southeast Indian Ocean. Combined U/Th, ^{14}C, and ε_{Nd} records were determined from the carbonate skeletons of both live and fossil corals collected from the Perth submarine canyon in the southeast Indian Ocean, offshore SW Australia (Fig. 1). Here, the corals spanned present-day water depths from 675 m to 1788 m and thus represent a depth transect through Subantarctic Mode Water, Antarctic Intermediate Water, and Upper Circumpolar Deep Water (Fig. 2). These records provide the first insights into recent (<2 ka) and glacial-early deglacial (~29–~17 ka) changes in ocean dynamics and uptake of atmospheric carbon and its transfer to mid-depth waters of the southeast Indian Ocean. With complementary foraminifer and coral records, we reveal abrupt, transient changes that can be correlated across the broader Southern Ocean region.

2. Oceanographic setting

The Perth Canyon (PC) is located along the passive continental margin approximately 50 km offshore Perth, Western Australia, and represents Australia's second largest submarine canyon system. The water masses filling the PC and offshore Perth Basin region comprise the Tropical Surface Water (TSW), South Indian Central Water (SICW), Subantarctic Mode Water (SAMW), Antarctic Intermediate Water (AAIW), Upper Circumpolar Deep Water (UCDW), Lower Circumpolar Deep Water (LCDW), and Antarctic Bottom Water (AABW) (Woo and Pattiaratchi, 2008; McCulloch et al., 2017; Trotter et al., 2019).

The SAMW, AAIW, UCDW, LCDW and AABW all form in the Southern Ocean and, apart from the LCDW and AABW, shoal northwards towards the Indian Ocean. The pathways of these water masses into the southeast Indian Ocean are longer than the Central and Western Indian Ocean sectors (Fig. 2). AABW, mostly sourced from the Ross Sea and Adélie Coast, flows northwest along a circuitous topographic path along the abyssal regions of the Australian Antarctic Basin, southeast Indian Ridge, and South Australian Basin, then northwest into the Perth Basin (Orsi et al., 1999; Rintoul, 2007). LCDW is formed partly from poleward flowing NADW into the ACC and outcrops near Antarctica where it is

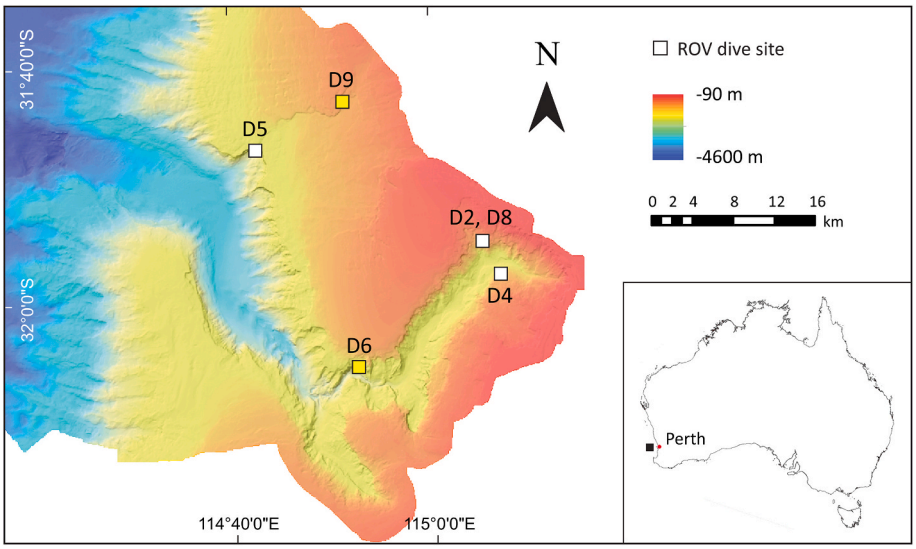

Fig. 1. Location of the Perth Canyon and ROV dive sites relevant to this study. Multi-beam sonar map incorporates new data from 2020 cruise (see text). Yellow squares represent last glacial coral sites. Dive site numbers D2 and D8, D4, D5, D6 and D9 relate to sites A, B, E, C, and F respectively from Trotter et al. (2019). (For interpretation of the references to colour in this figure legend, the reader is referred to the Web version of this article.)

transformed to AABW (Rintoul and Naveira Garabato, 2013). NADW also flows into the deep Indian and Pacific basins where via diapycnal mixing it contributes to the formation of UCDW, which upwells within the eastward flowing ACC (Rintoul and Naveira Garabato, 2013). The surface layer of upwelled recirculating UCDW is converted into less dense AAIW and SAMW which ventilate the upper ocean as they flow northwards (Rintoul and Naveira Garabato, 2013). Offshore southwest Australia, AAIW and SAMW also incorporate signatures from waters further east from around Tasmania transported by the Flinders Current (Fine, 1993; Wong, 2005). This current system originates near Tasmania and flows westwards along the South Australian margin. The Leeuwin Undercurrent off Western Australia is considered a northern extension of the Flinders Current (Woo and Pattiaratchi, 2008), which thereby promotes inter-ocean circulation between the South Pacific and southeast Indian oceans.

The hydrodynamics in and around the upper reaches of the PC is mostly influenced by this northward-flowing subsurface Leeuwin Undercurrent (~350–~800 m), which carries cooler, less saline, and high oxygen SAMW (>300–~750 m), and the overlying surface waters of the Leeuwin Current (LC; upper 300 m). The Leeuwin Current is a warm, oligotrophic, poleward-flowing eastern boundary current system, which transports nutrient-poor TSW (upper ~100 m) from the tropics together with cooler and higher salinity SICW (~100–~300 m) along the Western Australian margin. Interactions of the Leeuwin and Flinders current systems, however, fluctuate due to seasonal changes in their strength and hence geographic range along the west and south Australian margins (Woo and Pattiaratchi, 2008).

The SAMW (>300–~750 m), the low salinity AAIW (~750–~1000 m), and the low oxygen UCDW (~1000–~2000 m) span the depth ranges of the corals analysed in this study. The sources and pathways of these water masses in the canyon are controlled by three current systems, the ACC, and associated oceanic fronts and westerly winds that drive their eastward migration, as well as the Leeuwin Undercurrent and Leeuwin Current described above, which influence local upwelling, nutrient content, and oxygenation within surface and intermediate depths (Woo and Pattiaratchi, 2008; Rennie et al., 2009). Chlorofluorocarbon tracing indicates that AAIW in the southeast Indian Ocean is older (~30 years) than the more ventilated AAIW in the central Indian Ocean (~9 years), reflecting its longer pathway into the eastern sector (Fine, 1993; Wong, 2005).

3. Material and methods

3.1. Deep-water coral sampling

Deep-water scleractinian corals were collected in 2015 during cruise FK20150301 (McCulloch et al., 2017), from within and around the Perth Canyon (31°42′S–32°10′S and 114°42′E–115°05′E) using a Sub-Atlantic Comanche Remotely Operated Vehicle launched from the Schmidt Ocean Institute's R/V Falkor. The samples were collected from five dive sites between water depths of 675 m and 1788 m, from near the SAMW-AAIW boundary to UCDW (Figs. 1 and 2; Supplementary Table 1) (McCulloch et al., 2017; Trotter et al., 2019). The corals analysed and reported here are represented by both solitary (*Desmophyllum dianthus*, *Caryophyllia* sp., *Polymyces* sp.) and colonial (*Solenosmilia variabilis*) species. Live and recently dead specimens (<2000 years) were mostly sampled from the canyon walls at various depths and sites. Glacial subfossils were collected from two coral graveyard deposits separated by ~1000 m in water depth and located at each end of the study area: (1) in the southeast corner of the canyon (dive 6) partly buried in fine sediments between 1558 and 1788 m, and (2) along the northernmost survey site above the canyon (dive 9) where fossil corals covered the substrate between 691 and 746 m. Paired U/Th and radiocarbon ages were determined from the aragonite skeleton of 31 corals to establish absolute ages, 17 of which underwent Nd isotope analysis to assess changes in ocean dynamics (Supplementary Tables 2–4). These were selected as the best preserved specimens from approximately 50 recently dead and fossil solitary corals (including fragmented individuals) collected from 8 collection intervals, and scoops of colonial debris from six intervals.

3.2. U-series and radiocarbon dating

The corals were processed and analysed following conventional methods that are briefly outlined below with specific details given in the online Supplementary Material.

Sample preparation followed routine procedures. Corals were physically cleaned using a dental drill under a stereo microscope then crushed for chemical processing. Subsamples were split into ~5–20 mg aliquots for radiocarbon analysis and ~20–50 mg for absolute U-series dating. Samples for U/Th analysis were spiked with U and Th tracers (^{229}Th, ^{233}U and ^{236}U) and processed through Eichrom UTEVA ion

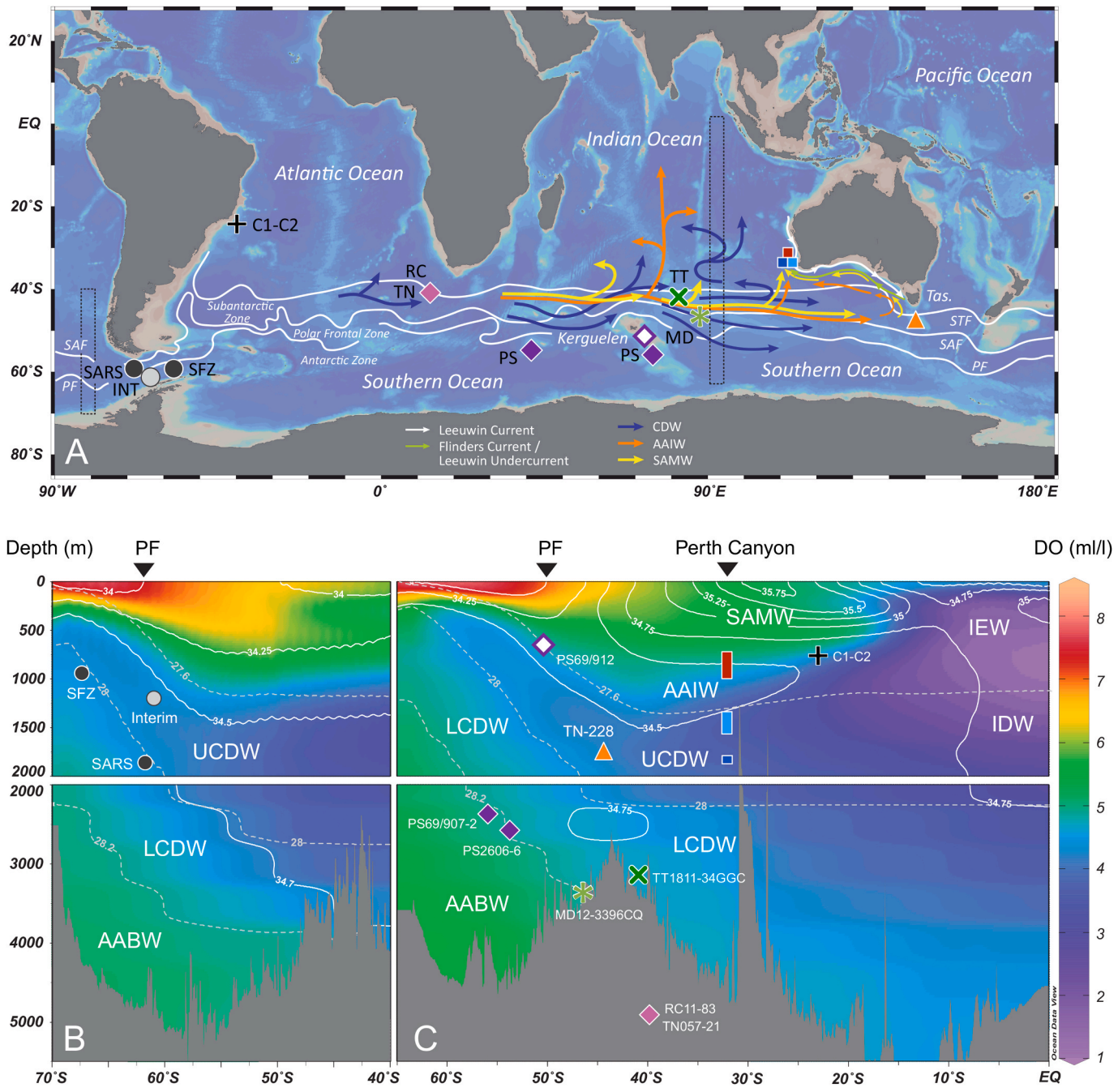

Fig. 2. (A) Map showing circulation pathways for mid and deep waters entering the Indian Ocean, circumpolar ocean fronts, southwest Australian currents, and locations of sample sites including published studies discussed in the text. Drake Passage corals: SFZ = Shackleton Fracture Zone, SARS = Sars Seamount, INT = Interim Seamount (Wilson et al., 2020); South Atlantic cores: RC11-83, TN057-21 (Piotrowski et al., 2008); Brazil cores: C1: ENG-111, C2: 21210009 (Mangini et al., 2010); Kerguelen cores: TT1811-34GGC (Williams et al., 2021), PS2606-6, PS69/907-2, PS69/912-3 (Ronge et al., 2020) and MD12-3396CQ (Gottschalk et al., 2020); as well as corals offshore Tasmania: TN228-J2 (Hines et al., 2015). STF = Subtropical Front, SAF = Subantarctic Front, PF = Polar Front. Dotted rectangles indicate the position of the sewater profiles in panels B and C. (B) Dissolved oxygen seawater profile along a latitudinal section in the Drake Passage. (C) Dissolved oxygen seawater profile along a latitudinal section across the central southern Indian Ocean and Southern Ocean. SAMW = Subantarctic Mode Water, IEW Indian Equatorial Water, AAIW = Antarctic Intermediate Water, UCDW = Upper Circumpolar Deep Water, IDW = Indian Deep Water, LCDW = Lower Circumpolar Deep Water, AABW = Antarctic Bottom Water. White lines denote salinity contours. Light grey dotted lines denote isoneutral contours (γ^N = 27.6 kg m^{-3}, 28 kg m^{-3}, 28.2 kg m^{-3}).

exchange chromatography resin to separate U and Th. U and Th isotope ratios of the sample solutions were measured using a Thermo Scientific Neptune Plus MC-ICPMS at the Advanced Geochemical Facility for Indian Ocean Research at the University of Western Australia. CRM112-A and IRMM-363a standard reference materials were used to correct for analytical bias. Ages were calculated through iterative age estimation and assuming a $^{232}Th/^{230}Th$ ratio of 14.8 for detrital correction, then calibrated to the year 1950 (i.e. BP). Aliquots for radiocarbon analyses were processed by the GEOTRAC Team at the Laboratoire des Sciences du Climat et de l'Environnement (LSCE), Gif-sur-Yvette, France. The carbonate was converted to CO_2, with large samples reduced to graphite and measured at the AMS-ARTEMIS facility. CO_2 collected from the small samples were measured via the gas ion source of the AMS ECHoMICADAS.

Reconstructed palaeoseawater radiocarbon is expressed as conventional delta permil notation $\Delta^{14}C$ (‰), calculated from the measured U/Th and ^{14}C ages of the corals. The $\Delta^{14}C_{DWC}$ values were also converted to epsilon units (ε) to effectively compare seawater and contemporaneous atmosphere $\Delta^{14}C$ compositions, accounting for temporal changes in atmospheric $\Delta^{14}C$. Benthic-atmosphere (B-Atm) ages were calculated as the difference between coral and contemporaneous atmospheric ^{14}C ages (i.e. based on U–Th age) to determine the deep-water ventilation age at each location. Radiocarbon data of modern seawater samples from the coral collection sites are described and reported in Trotter et al. (2019). Present-day seawater radiocarbon is compared with ^{14}C compositions measured from modern corals from various depths and used to validate inferred temporal differences in seawater radiocarbon recorded by fossil corals.

3.3. Neodymium isotope analysis

Samples were prepared and analysed following conventional techniques that are briefly outlined below, with specific details given in the online Supplementary Material. Corals selected for Nd isotope analysis underwent the same physical cleaning and pre-dissolution protocol as used for U/Th processing. Large subsamples were required (~200–300 mg) which limited the coral material available for analysis. Nd was separated using a 2-tiered chromatography procedure containing TRU Spec and LN resins. Three samples not previously dated were first processed using the U/Th ion exchange procedure, the eluent then processed using the Nd separation protocol (see Supplementary file). Nd isotope ratios of the sample solutions were measured using a Thermo Scientific Neptune Plus MC-ICPMS at the Advanced Geochemical Facility for Indian Ocean Research at the University of Western Australia. The samples were normalised to the La Jolla bracketing standard reference material. Data are expressed in epsilon units, referenced to the present-day composition of the Chondritic Uniform Reservoir.

4. Results

The U/Th ages (Supplementary Table 2; Fig. 3) of the deep-water corals analysed fall into two main time intervals. A younger subset of fossil and live samples ranges from ~2 ka BP to present, and those within the last glacial period and early deglaciation from 29.6 to 17.5 ka BP, through Marine Isotope Stage 2 (MIS 2), thus spanning Heinrich Stadial 2 (HS2), the Last Glacial Maximum (LGM), and initiation of Heinrich Stadial 1 (HS1), the latter typically considered the onset of deglaciation (~18 ka). The modern and glacial corals were collected from similarly wide depth ranges, of ~675–~1558 m and ~691–~1788 m respectively, enabling comparison of samples from deep (UCDW) and overlying intermediate waters (SAMW to AAIW) for both time intervals. Acknowledging the uncertainty associated with an ~120 m sea level fall during the LGM, the shallower glacial corals might have grown within SAMW or transitional SAMW-AAIW depths during this period, so are hereon discussed in that context. The age ranges of HS2 (27-24 ka), the LGM (24-18 ka), and HS1 (18–14.6) used follow Burke and Robinson (2012), however definitions of these intervals vary greatly within the literature.

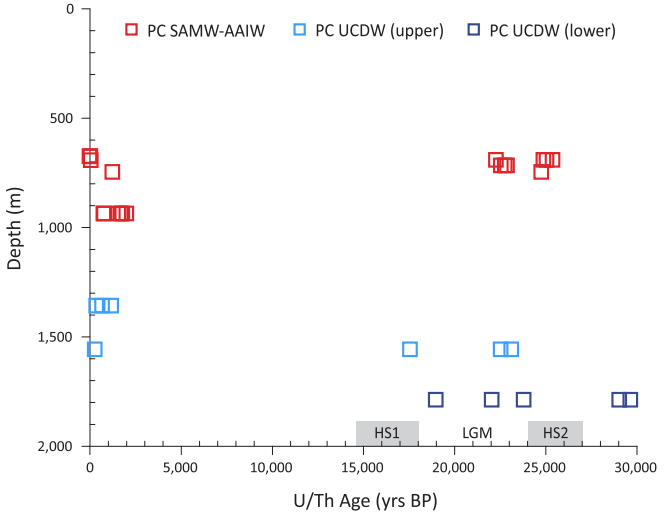

Fig. 3. U/Th age versus depth of Perth Canyon glacial and modern corals. Glacial corals are from dive sites 6 (UCDW) and 9 (SAMW-AAIW). For further details see Supplementary Table 2. HS = Heinrich Stadial, LGM = Last Glacial Maximum.

Radiocarbon ages (Supplementary Table 3) of the glacial corals range from 26 to 14.9 ka BP and Holocene ages span years 2.6 to 0.13 ka BP. Calculated $\Delta^{14}C_{DWC}$ values fall between +481 and −169‰ (Supplementary Table 3; Fig. 4A), which are below the Southern Hemisphere $\Delta^{14}C_{ATM}$ atmosphere curve (SHCal20) at their respective ages. Although the range of $\Delta^{14}C_{DWC}$ values from glacial SAMW-AAIW corals (481–251‰) broadly overlap with those from the UCDW (419–210‰), they are only temporally equivalent at ~23 ka and within shallower depths (upper UCDW at 1558 m). Only deeper UCDW (1788 m) seems compositionally lower, acknowledging no temporal equivalence with SAMW, AAIW, and upper UCDW. The absolute offset between the glacial corals and contemporaneous atmospheric radiocarbon compositions (calculated in epsilon units) reveals significant temporal variability within SAMW-AAIW and UCDW water masses, being negatively offset by ~40 to ~200‰ (Fig. 4B; Supplementary Table 3). Most notable, is the sudden large decrease in glacial SAMW-AAIW radiocarbon by ~140‰ (from −54 to −197 epsilon ‰) at 25 ka, which occurred over a short time interval of ~300 years. This shift translates to a sudden increase in the water mass ventilation age by 1315 years, expressed as B-Atm (yrs), calculated as the difference between atmosphere and coral ^{14}C ages (see Discussion).

Holocene $\Delta^{14}C_{DWC}$ values (−21 to −169‰) are considerably lower than the glacial radiocarbon compositions, reflecting the systematic decline in $\Delta^{14}C_{ATM}$. The few Holocene UCDW corals have somewhat lower $\Delta^{14}C_{DWC}$ (−117 and −169‰) than AAIW corals (−21 and −133‰), with the latter showing little variation (−107 to −133‰) between ~1800 and ~700 years BP but significantly higher values (−21 to −83‰) close to the atmosphere curve for those younger than 30 years BP (Supplementary Table 3, Fig. 4); this excludes the potentially anomalous high ^{232}Th sample (~2 ka BP, $\Delta^{14}C_{DWC}$ = −85‰). Two corals of similar ages representing each water mass, year ~1150 (upper UCDW, 1357 m) and ~1200 (AAIW, 746 m), have similar $\Delta^{14}C_{DWC}$ values (−117 and −107 respectively). Although the few younger UCDW corals (n = 3) between ~250 and ~650 years BP yielded measurably lower values, there are no contemporaneous AAIW corals to determine potential relative differences in radiocarbon compositions between these water masses. The radiocarbon offset of Holocene corals relative to the atmosphere curve is within −40 and approximately −160 epsilon ‰ (Fig. 4B). Notably, the radiocarbon compositions of two live corals collected from AAIW ($\Delta^{14}C_{DWC}$ = −21, −57‰) and the youngest UCDW corals dated at ~250 and 330 yr BP ($\Delta^{14}C_{DWC}$ = −142, −169‰) compare well with present-day seawater $\Delta^{14}C$ measurements of −35‰ at ~675 m and −170‰ at 1357 m (Supplementary Tables 1 and 3). We also note that $\Delta^{14}C$ measurements of present-day deep UCDW at 1790 m (−185‰), equivalent to seawater $\varepsilon^{14}C$ of −167‰, is very close to glacial $\varepsilon^{14}C$ at this depth (−172, −180 at ~22–24 ka) and thus have equivalent ventilation ages of 1580 yrs and 1500-1600 B-Atm yrs respectively. Conversely, deep UCDW $\varepsilon^{14}C$ during early deglacial conditions (18.9 ka) and especially early MIS 2 (29.6 ka) are closer to contemporaneous atmosphere (−131‰ and −79 respectively) hence considerably more ventilated.

ε_{Nd} values determined from a selection of modern and glacial corals from SAMW-AAIW and UCDW depths range between −5.6 and −8.4 (Supplementary Table 4; Fig. 5). The glacial SAMW-AAIW corals

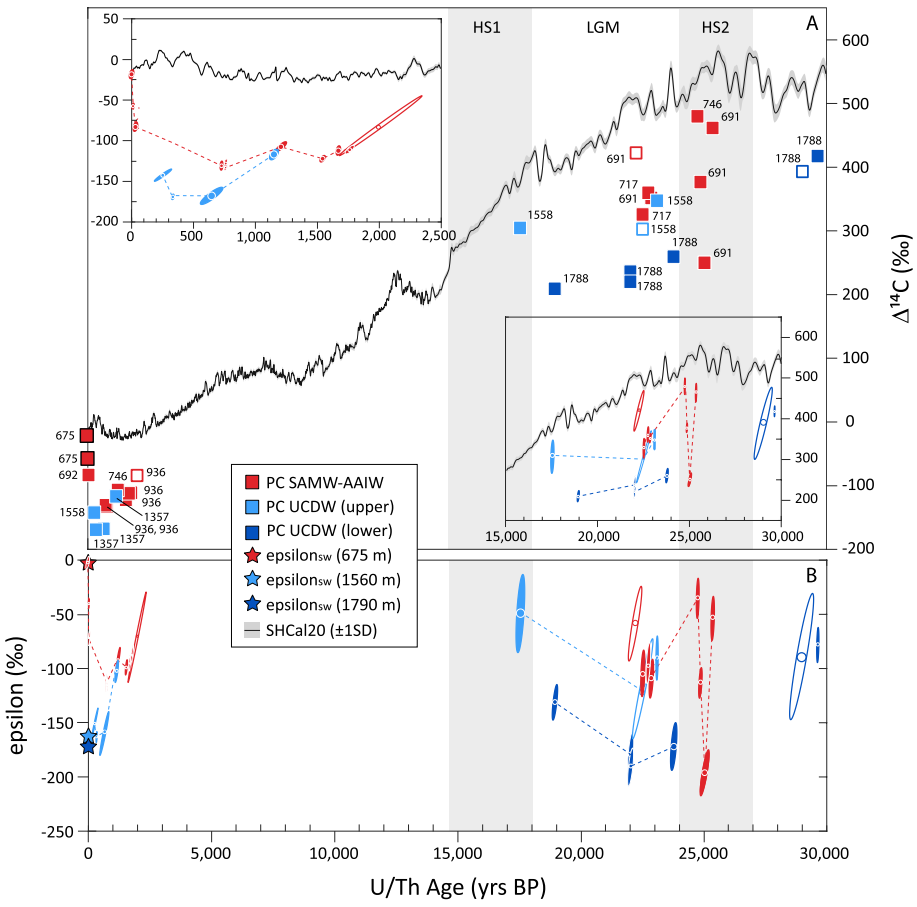

Fig. 4. U/Th age versus $\Delta^{14}C$ of Perth Canyon corals, ambient seawater, and contemporaneous atmosphere (A). Coral epsilon ^{14}C shown with error ellipses (B). Squares with black outline denote live corals. Empty squares and error ellipses denote samples with high ^{232}Th (i.e. 2-3 ppb). Seawater $\Delta^{14}C$ from Trotter et al. (2019), $\Delta^{14}C$ atmosphere curve (SHCal20) is the Southern Hemisphere calibration from Hogg et al. (2020). Numbers with data symbols are sample collection depths in metres. HS = Heinrich Stadial, LGM = Last Glacial Maximum.

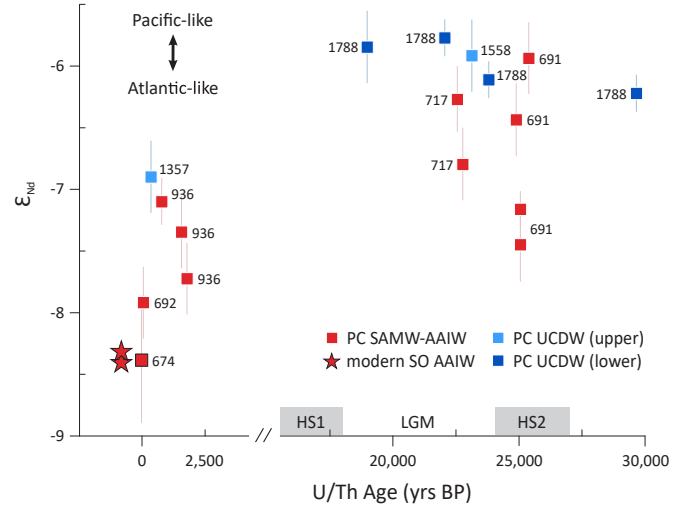

Fig. 5. U/Th age versus ε_{Nd} of Perth Canyon glacial and modern corals. Present-day Southern Ocean AAIW ε_{Nd} (stars) from Lambelet et al. (2018). Square with black outline denotes live coral. Numbers with data symbols are sample collection depths in metres. Uncertainties plotted at 2σ (95% confidence limits). HS = Heinrich Stadial, LGM = Last Glacial Maximum.

(25.4–22.5 ka BP) have ε_{Nd} compositions between −5.9 and −6.8, except one coral from ~25 ka BP that repeatedly yielded measurably lower values (−7.2 and −7.4), reflecting a sudden drop by ~1.5 epsilon units. This coral also yielded a very low radiocarbon composition relative to atmosphere (−196 $\varepsilon^{14}C$ ‰), thereby recording a concomitant decline in both Nd isotope and radiocarbon in SAMW-AAIW at ~25 ka.

The deeper corals from UDCW span a longer age interval (29.6–18.9 ka BP) yet have consistent ε_{Nd} values, from −5.6 to −6.2. The youngest PC corals (<1.8 ka) yielded ε_{Nd} compositions between −6.9 and −8.4, which are lower than most of the glacial corals. Of the modern samples, the highest ε_{Nd} value (−6.9) was determined from the deepest (UCDW) young sample, and the lowest (−8.4) from the live coral collected from AAIW; these represent the lowest measured ε_{Nd} compositions for these water masses from all corals analysed.

Overall, within a given water mass, our coral records show greater variability in radiocarbon throughout MIS 2 and the LGM together with more radiogenic (Pacific-like) ε_{Nd} values compared to the recent interval (<2 ka). The glacial SAMW-AAIW and UCDW data sets overlap, with UCDW showing little variability and slightly higher ε_{Nd} values. The most striking observation is the concomitant rapid decline then recovery in both $\Delta^{14}C_{DWC}$ and ε_{Nd} within glacial SAMW-AAIW at ~25 ka.

5. Discussion

5.1. Comparison of modern coral and seawater compositions

Data from the modern PC corals are consistent with known circulation and ventilation patterns of present-day mid to deep waters around the Southern Ocean. The radiocarbon and ε_{Nd} records of live and recently dead canyon corals are compatible with ambient seawater ^{14}C measurements (Fig. 4) and ε_{Nd} compositions typically reported for the modern Southern Ocean (e.g. Piepgras and Wasserburg, 1980; van de Flierdt et al., 2016; Tachikawa et al., 2017; Lambelet et al., 2018, Fig. 5). Unfortunately, there are no mid or deep water ε_{Nd} data from the higher latitudes across the southeast Indian Ocean, however further east from the Indo-Pacific Southern Ocean region south of Tasmania (Lambelet et al., 2018), AAIW has ε_{Nd} values of −8.3 (SR3-GIPY6-42) and −8.2

(SR3-GIPY6-60) thus equivalent to our PC live coral composition of −8.4 (Fig. 5). An estimate of mean ε_{Nd} Indian Ocean seawater of −8.4 is based on a consistent depth profile between 305 and 4505 m around Madagascar (Bertram and Elderfield, 1993), whereas recent mean estimates for southern Indian Ocean CDW and AAIW (−7.9 and −7.6 respectively) given by Tachikawa et al. (2017) are slightly higher. Notably, the southern Indian Ocean estimates are based on the NEOSYMPA database, which includes seawater measurements from mid to low latitudes from the eastern sector that are strongly influenced by more positive Pacific-sourced signatures via the Indonesian Throughflow; the few data at higher latitudes off SW Australia nearer our study region are limited to surface depths (~5 m).

The lower ε_{Nd} compositions of the modern and Holocene compared to glacial PC corals are also consistent with archives from other sites and ocean models (e.g. Skinner et al., 2013; Basak et al., 2018; Zhao et al., 2019; Du et al., 2020). Those data suggest that since the last deglaciation there has been greater mixing between deep and intermediate waters at Southern Ocean high latitudes with increased contributions of low ε_{Nd} Atlantic waters (e.g. Robinson and van de Flierdt, 2009). However, non-conservative effects (e.g. from changes in weathering particulate input fluxes in the North Atlantic during LGM) may also explain the more radiogenic Nd composition of the glacial ocean (Pöppelmeier et al., 2022).

5.2. Changes in glacial-interglacial ocean ventilation and circulation

Prior to the LGM, the PC SAMW-AAIW corals were seemingly exposed to waters with highly variable ε_{Nd} and radiocarbon compositions, implying dynamic oceanographic conditions operated during this interval (~26-23 ka). Previous studies have inferred that glacial Southern Ocean circulation was not always in steady state, based on millennial and centennial scale variability in foraminifer and coral records of mid to deep waters near the Subtropical and Subantarctic Fronts (STF, SAF), at sites upstream and downstream from the PC (e.g. Williams et al., 2021; Hines et al., 2015, Figs. 6 and 7). This is also supported by proxy records (grain size and composition) of ACC intensity near the Drake Passage during MIS 3 and 2, which have revealed high amplitude millennial-scale fluctuations in the lead up to the LGM (Wu et al., 2021, Fig. 8C).

The coral radiocarbon data for glacial PC SAMW-UCDW is largely consistent with that of contemporaneous corals collected from Southern Ocean AAIW offshore Tasmania (Hines et al., 2015), southeast Australia (Fig. 6); however we note their location nearer to the present-day AAIW-UCDW boundary (Fig. 2B). The similarities of age equivalent samples between the PC and Tasman records imply that these water masses have common ventilation histories, although the absence of Tasman ε_{Nd} records precludes tracing source water origins. Given that AAIW shoals as it flows northward, PC glacial SAMW-AAIW corals should have been exposed to similar Southern Ocean-derived waters to those at the deeper and higher latitude Tasman site. Furthermore, the overall consistent compositions between PC SAMW-AAIW and the upper portion of UCDW, evident from coeval corals at ~23 ka from disparate depths (~700 and 1558 m, Fig. 4), suggest that during this time these waters were essentially homogenous over a wide depth range.

PC deep UCDW (1788 m) and Tasman AAIW-UCDW were highly ventilated during early MIS 2 (659 years at 29.6 ka and 259 years at 27.6 ka respectively), much more than present-day UCDW (~1400 B-Atm years; Fig. 6). Highly ventilated PC UCDW coincided with reduced Antarctic sea-ice and warmer temperatures, as well as a stronger AMOC (Fig. 8). However, during the LGM at ~22–24 ka, deep UCDW (1788 m) had a ventilation age of ~1500–1600 yrs thus equivalent to (or slightly older than) present-day seawater at this depth. Most evident and unusual, however, in both the glacial PC SAMW-AAIW (690 m) and Tasman AAIW-UCDW records is the large sudden drop in $\Delta^{14}C_{DWC}$ at ~25 ka by ~210‰ and ~125‰, corresponding to an increase in B-Atm ventilation ages by ~1315 and ~765 years respectively. This implies

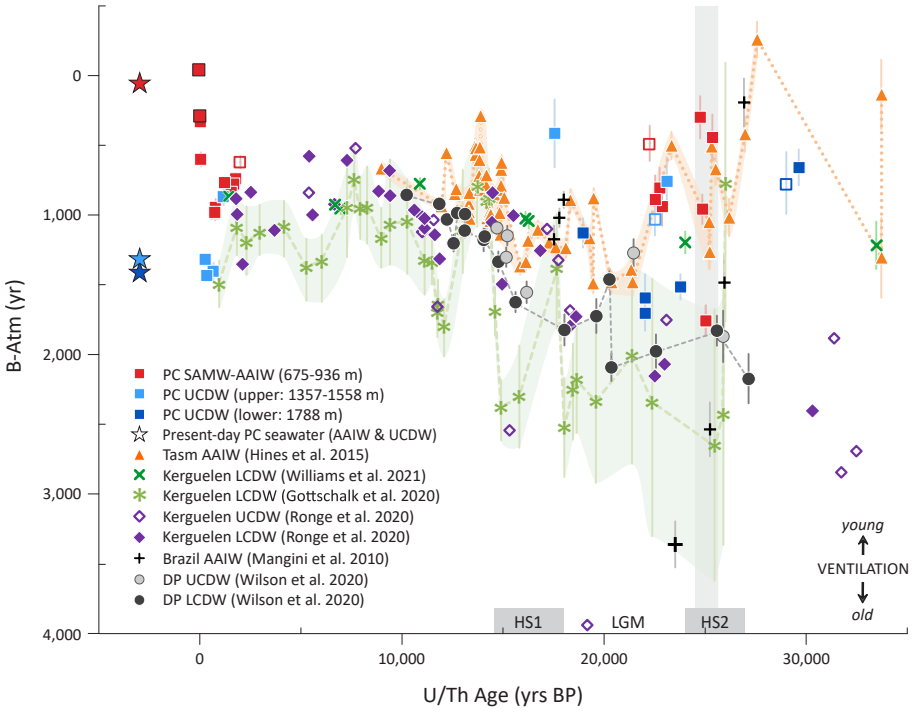

Fig. 6. U/Th age versus B-Atm of Perth Canyon SAMW-UCDW glacial and modern corals (squares: this study) and from the literature: Tasman AAIW corals (triangles: TN228, 1430–1950 m), Drake Passage U-LCDW corals (circles: Interim Seamount, 982–1196 m; Shackleton Fracture Zone, 806–823 m; Sars Seamount, 1701–1750 m), Brazil AAIW corals (black crosses: C1: ENG111, 621 m; C2: 21210009, 781 m), foraminifers from Keguelen UCDW (purple open diamonds: PS69/912-3, 567 m) and LCDW (green crosses: TT181-34GGC, 3167 m; olive asterisk: MD12-3396CQ, 3615 m; purple filled diamonds: PS2606-6, 2545 m; PS69/907-2, 2253 m). Squares with black outline denotes live corals; open squares denote high 232Th data (2–3 ppb). Present-day Perth Canyon seawater B-Atm ages for AAIW (red star: 675 m) and UCDW (light and dark blue stars: 1560 and 1788 m) increase with depth; calculated from Trotter et al. (2019). Orange and green and bands encompass the uncertainty minima-maxima for the most comprehensive records of Hines et al. (2015) and Gottschalk et al. (2020). B-Atm ages are calculated using the SHCal20 ^{14}C atmosphere calibration curve, except data from Gottschalk et al. (2020) and Ronge et al. (2020) which are based on InterCal13. Uncertainties are calculated using the quadratic sum of the ^{14}C sample and atmosphere ages and are given at 1σ (66% confidence limits). Data of Ronge et al. (2020) based on the recalculated B-Atm ages from Gottschalk et al. (2020) with no errors reported. HS = Heinrich Stadial, LGM = Last Glacial Maximum. (For interpretation of the references to colour in this figure legend, the reader is referred to the Web version of this article.)

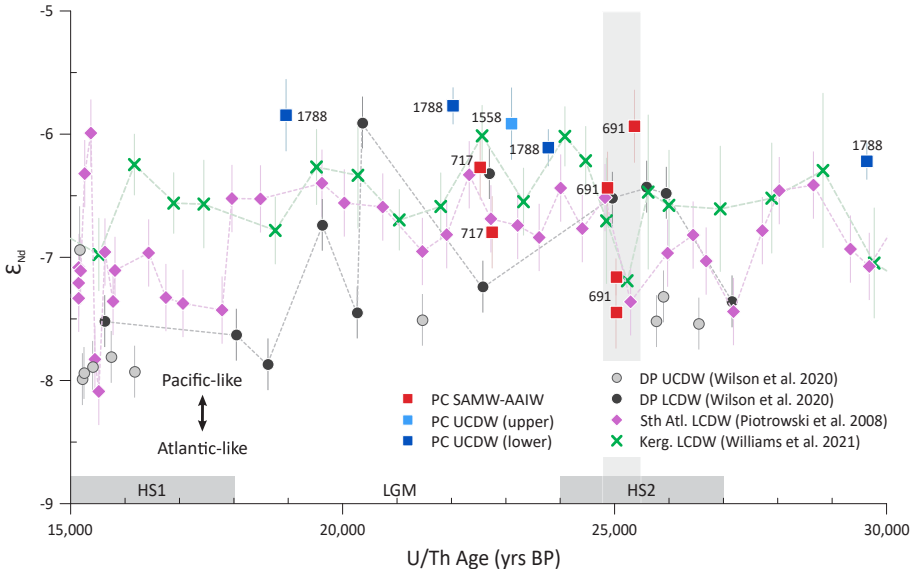

Fig. 7. U/Th age versus ε_{Nd} of Perth Canyon SAMW-UCDW glacial corals (squares: this study), Drake Passage CDW corals (circles: Wilson et al., 2020), Kerguelen foraminifers (crosses: Williams et al., 2021), and South Atlantic core sediments (diamonds: Piotrowski et al., 2008). Numbers against Perth Canyon data (squares) are sample collection depths in metres. Uncertainties plotted at 2σ (95% confidence limits). HS = Heinrich Stadial, LGM = Last Glacial Maximum. See Figs. 2 and 6 for site names, locations, and depths.

short-lived mixing with less ventilated waters within several hundred years (see section 5.3).

After the LGM, the PC and Tasman records diverge, with PC upper UCDW (1558 m) having a much younger ventilation age (B-Atm age ~400 yrs) at ~17.5 ka. Even the deepest PC interval at 1788 m decreased in B-Atm age to ~1130 yrs at ~19 ka BP, which was equivalent to Tasman AAIW-UCDW, compared to ~1600 yrs at ~22 ka BP (i.e. by ~470 yrs, Fig. 6). These considerably younger B-Atm ages imply that UCDW in the PC became ventilated, which coincides with Antarctic sea-ice retreat, warming, increasing atmospheric CO_2, and the southward shift of oceanic fronts thus consistent with the replacement of polar foraminifers by tropical species along SW Australia (Fig. 8). The deglacial offset between PC UCDW and Tasman AAIW-UCDW radiocarbon (414 and 1175 B-Atm yrs respectively at 17.5 ka) implies a change in intermediate and circumpolar hydrodynamics across the Indo-Australian Southern Ocean. Although we have no reason to doubt their integrity, we acknowledge that these data are few so future studies would clarify the validity of these inferences.

Interestingly, the decrease in PC UCDW ventilation age by ~700 B-Atm years between 18.9 (1788 m) and 17.5 ka (1558 m), is of similar magnitude (~800 years) to that registered in Kerguelen SAF LCDW (MD12-3396CQ at 3615 m), the latter older than PC UCDW by ~900 B-Atm years. However, we highlight the different UCDW depths (1558 versus 1788 m) in PC, which likely influenced their radiocarbon compositions (partly if not entirely), noting the typically older ages at 1788 m depths albeit not strictly coeval with other samples. Unfortunately, the small size of the PC deglacial coral (~17.5 ka) precluded sampling for ε_{Nd} analysis so source water information is lacking.

Comparison of ventilation histories recorded at the Perth Canyon, Kerguelen, and Drake Passage sites is limited by the sparse temporal overlap of these records, nevertheless some similarities are apparent. At ~24 ka, the ventilation age of deep PC UCDW (1788 m) is similar but older than STF LCDW north of Kerguelen (TT1811-34GGC: Williams et al., 2021). At 22 ka, deep PC UCDW ventilation ages lie between Drake Passage UCDW (21.5 ka; equivalent to Tasman AAIW-UCDW boundary) and LCDW (22.5 ka) (Figs. 6 and 8B). Sites further south and west within the Polar Front, near Kerguelen and Conrad Rise (Ronge et al., 2020, B-Atm calculated by Gottschalk et al., 2020 using their reservoir age constraints), generally show similar less ventilated ages most like LCDW at the Drake Passage (Fig. 6). We note that the Kerguelen record near the present-day SAF (core MD12-3396CQ: Gottschalk et al., 2020) might appear significantly less ventilated than the STF LCDW (Williams et al., 2021), however data from the latter are sparse. Considering their different locations, latitudinal displacement of the westerly winds and associated ACC and oceanic fronts (possibly from ~3 to 10° or more, see Toggweiler et al., 2006; Kohfeld et al., 2013; De Deckker et al., 2012, 2020) due to migrating sea-ice might impart different oceanic signals at the southern and northern Kerguelen sites, consistent with bathymetric controls on the ACC by the Kerguelen Plateau (van Wijk et al., 2010). The absence of ε_{Nd} data from the southern Kerguelen SAF and PF LCDW (MD and PS cores) and limited radiocarbon data from Kerguelen STF LCDW precludes further comparison between these sites.

5.3. *A brief widespread oceanographic event at 25 ka*

The PC shows a concomitant shift to lower $\Delta^{14}C$ and more Atlantic-like unradiogenic ε_{Nd} composition at 25 ka, followed by rapid recoveries in both radiocarbon and ε_{Nd} (Fig. 8A and B). Comparisons of our paired $\Delta^{14}C_{DWC}$–ε_{Nd} glacial data with published radiocarbon and ε_{Nd} records (Figs. 6, 7, 8A-B) from Drake Passage CDW corals (Wilson et al., 2020), LCDW foraminifers near Kerguelen (Gottschalk et al., 2020; Williams et al., 2021), and sediments from the southeast Atlantic (Piotrowski et al., 2008), provide insights into hydrodynamic links between these geographically disparate sites. The distinct ε_{Nd} minimum then sudden rise around 25 ka in PC SAMW-AAIW, Kerguelen STF LCDW, and southeast Atlantic LCDW (Fig. 8A), indicate widespread circumpolar intermediate water connectivity around the Southern Ocean at this time. Consistent with the PC SAMW-AAIW radiocarbon data, both the Tasman AAIW-UCDW and Kerguelen SAF LCDW (core MD12-3396CQ) also show a sudden change to poorly ventilated waters at ~25 ka (Figs. 6 and 8). Prior to this event, the oldest Kerguelen datum is well ventilated, similar to the Tasman record, with AAIW off Brazil (Mangini et al., 2010) also showing a large change in ventilation age. However, we acknowledge the large uncertainties associated with the ventilation ages of the Kerguelen record. Furthermore, cross-plots showing the relationship of ventilation age and ε_{Nd} of the few available paired $\Delta^{14}C$–ε_{Nd} data sets (Fig. 9), suggest glacial source water links where PC and Kerguelen STF LCDW data overlap, these fields being distinct from the high-latitude Drake Passage glacial CDW. The notable exception, however, is PC SAMW-AAIW at ~25 ka that plots well within the broader domain of the less ventilated and less radiogenic (lower) ε_{Nd} Drake Passage data.

The consistent and transient behaviour of both ε_{Nd} and water mass aging indicate rapid (centennial-scale) and distinct shifts in ocean chemistry, suggesting that a sudden pulse of older poorly ventilated deep water with Atlantic affinities was injected into overlying

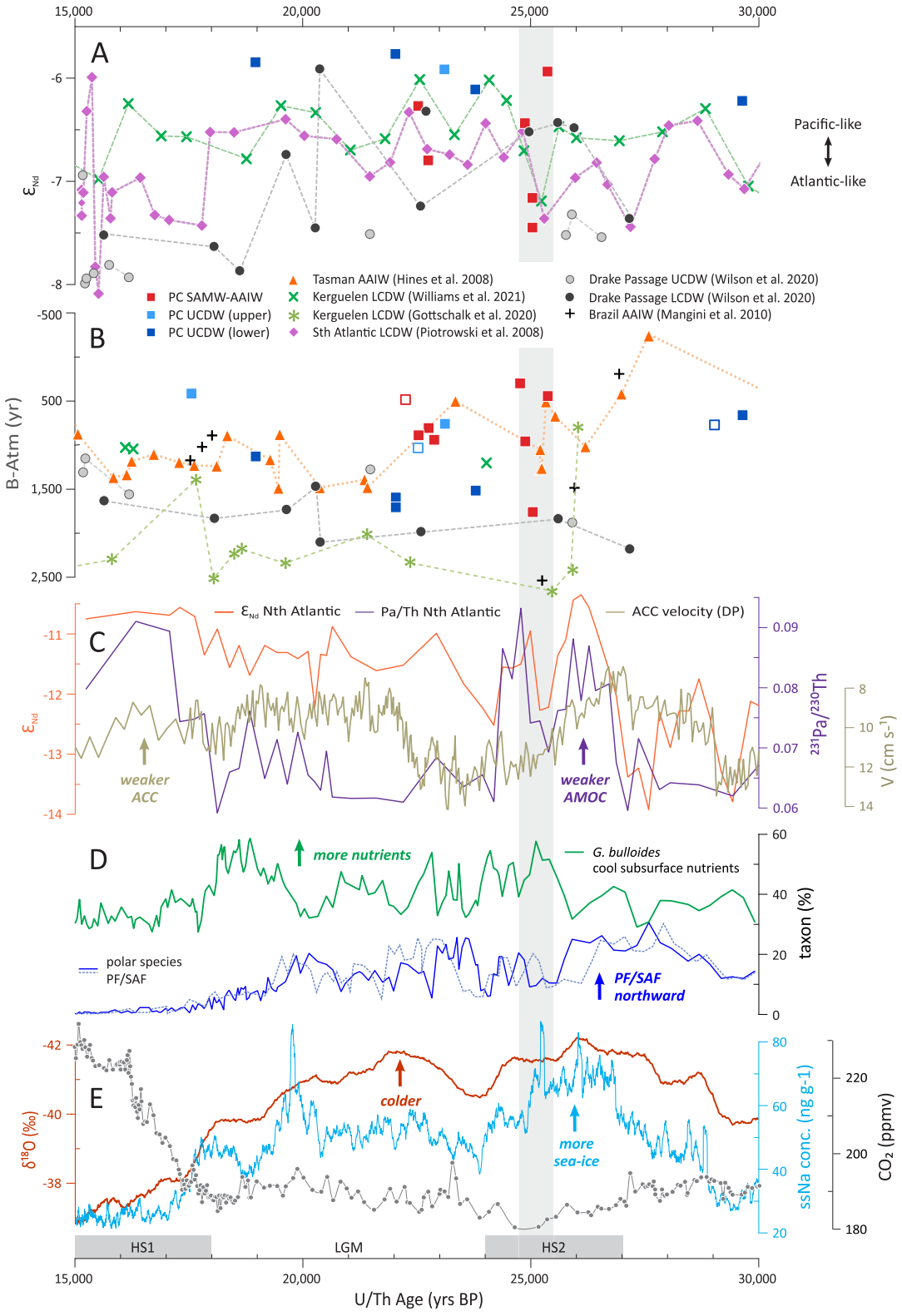

Fig. 8. Composite of proxy records for 15,000 to 30,000 years BP discussed in the text. (A) U/Th age BP versus ε_{Nd} of Perth Canyon SAMW-UCDW corals (squares: this study), Drake Passage corals, Kerguelen foraminifers, and South Atlantic core sediments; (B) B-Atm records from Perth Canyon, Tasman, Drake Passage, and Brazil corals and Kerguelen foraminifers; (C) Paired Nth Atlantic Bermuda Rise ε_{Nd} and Pa/Th records (Böhm et al., 2015), and ACC Nd velocity (axis reversed) at the Drake Passage based on sortable silt percentages (Wu et al., 2021); (D) foraminifer species percentages from southern Australia indicative of oceanic front movements and subsurface upwelling (dashed line: De Deckker et al., 2012; solid lines: De Deckker et al., 2020); and (E) West Antarctic Ice Sheet Divide Core 06A ssNa and $\delta^{18}O$ (at 30 per moving average with axis reversed; WAIS Divide Project WAIS 2013 Divide Project Members, 2013, 2015); and composite CO_2 record from WAIS and Siple Dome (Bereiter et al., 2015). HS = Heinrich Stadial, LGM = 2 Last Glacial Maximum. Open squares denote data with higher ^{232}Th concentrations (2–3 ppb), slightly above the commonly acceptable range of ≤2 ppb (see Supplementary methods), yet are comparable to low ^{232}Th data. See, Figs. 2 and 6 for sample locations, depths and citations.

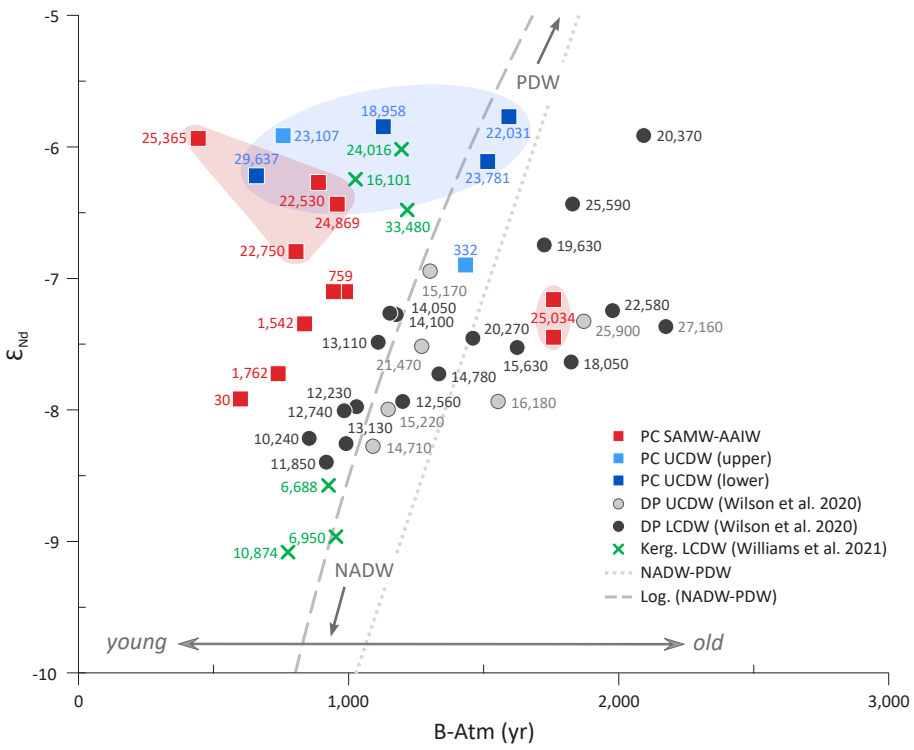

Fig. 9. B-Atm versus ε_{Nd} compositions of glacial and modern corals from the Perth Canyon (squares: this study) and Drake Passage (circles: Wilson et al., 2020), and foraminifers from Kerguelen cores (crosses: Williams et al., 2021). Note the distinctly different composition for Perth Canyon SAMW-AAIW data at 25 ka data falls within the older and lower ε_{Nd} field typical of Drake Passage CDW. Dashed line defined by end-member compositions of North Atlantic Deep Water and Pacific Deep Water (from Struve et al., 2020). Numbers against data symbols are sample ages (yr BP). Red and blue fields encompass Perth Canyon SAMW-AAIW and UCDW data sets respectively for the LGM. B-Atm ages are calculated using the SHCal20 ^{14}C atmosphere calibration curve.

intermediate waters. A rapid recovery is also shown in the three ε_{Nd} records, at the southeast Atlantic, Kerguelen STF, and Perth Canyon sites, the ventilation history at the latter indicating a shift to more ventilated conditions within ~300 years.

Although the poorly ventilated glacial $\Delta^{14}C_{DWC}$ and less radiogenic ε_{Nd} values are represented by only one PC coral, the replicate ε_{Nd} measurements (−7.5, −7.2) and consistent pattern between different archives from disparate sites (Figs. 7 and 8A) substantiate these data. We also deduce that this transient ε_{Nd} shift is not likely related to boundary exchange with the local Perth Basin geology given the rocks in this area have significantly higher epsilon values (approximately ≥ −3; Champion, 2013).

5.4. *Processes influencing circumpolar hydrography*

The sudden, brief (~300 yrs) decline in PC glacial SAMW-AAIW ε_{Nd} composition by ~1.5 units together with water mass aging by ~1300 years at 25 ka (Fig. 8A–B), requires the injection of considerably older (less ventilated) deep water with a more Atlantic-like (less radiogenic) low ε_{Nd} signature into mid-depth waters. This combination of poorly ventilated and lower ε_{Nd} composition is, however, unexpected given the world's least ventilated waters generally emanate from the deep Pacific Ocean which have higher, not lower, ε_{Nd} values. A shift to more negative ε_{Nd} values implies that the relative contributions of the Nd isotopic end-members, Pacific Deep Water (PDW) and North Atlantic Deep Water (NADW), transported into the Southern Ocean switched to favour NADW due to either increased production, and/or physical changes in water mass interactions within the ACC. Other proxy records also reveal significant and sudden changes around 25 ka in NADW production and AMOC strength, as inferred from paired ε_{Nd} and $^{231}Pa/^{230}Th$ records from the northwest Atlantic (Böhm et al., 2015), and West Antarctic sea-ice cover deduced from sea-salt sodium concentrations (ssNa: WAIS 2013 Divide Project Members, 2013; 2015) (Fig. 8C and E). West Antarctica registered the most extreme conditions during this period, with both sea-ice maximum and temperature ($\delta^{18}O$: WAIS 2013 Divide Project Members, 2013; 2015) minimum between ~27-25 ka, and lowest atmospheric CO_2 concentrations (Bereiter et al., 2015) at 25 ka reflecting an unventilated deep ocean and high carbon storage (Fig. 8). The ssNa record also indicates a brief peak then rapid decline in sea-ice cover from ~25 ka, at which time AMOC production, hence strength, had also peaked then weakened. We therefore argue that the 25 ka event reflects two processes: (1) a distinct increase in AMOC strength and NADW contributions into the Southern Ocean, and (2) an abrupt mode switch in circumpolar hydrography across the ACC.

Closer to our study site, changes in the abundance of (sub) polar and tropical foraminifer species (De Deckker et al., 2012, 2020) reflect fluctuations in ocean front positions, which migrated closer to the South Australian margin during the last glaciation. Based on the new age model reported by De Deckker et al. (2020), the SAF and STF temporarily retreated southward at around 25 ka, with foraminifer ecology also revealing a concomitant peak in cool-nutrient subsurface waters off South Australia (Fig. 8D). Fluctuations in diatom abundances in the southwest Atlantic and southwest Indian Ocean sectors of the Southern Ocean have also suggested declining sea-ice cover at this time (e.g. Xiao et al., 2016; Wu et al., 2021). Diatom-based Antarctic winter sea-ice minima have been correlated to ACC velocity maxima (estimated from sediment grain-size) in the Scotia Sea (Wu et al., 2021), implying that ACC strength was closely linked to Southern Hemisphere climate oscillations and sea ice cover (Fig. 8C and D).

Interestingly, at ~25 ka the midsummer Northern Hemisphere (65°N) insolation approaches its minimum which then switches to increase synchronously with Southern Hemisphere (65°S) midsummer insolation (nearing its maximum). This overlap of increasing insolation (i.e. enhanced energy received by both hemispheres), led by the Southern Hemisphere (Schulz and Zeebe, 2006), occurs from changes in orbital forcing (precession, obliquity, eccentricity) which is hypothesized as the trigger for the ensuing glacial termination, the onset of which is calculated at ~23 ka (Schulz and Zeebe, 2006). This forcing thus relates to the amount of energy supplied to each hemisphere, which influences ice melt and ultimately deep-water formation and global ocean circulation patterns (Schulz and Zeebe, 2006).

Both the pre-LGM event and early deglaciation registered in PC SAMW-AAIW and UCDW, co-occurred with Heinrich Stadials (HS), HS 2 and HS 1 respectively (Fig. 8). We note that intervals around HS,

especially those occurring close to glacial maxima, are linked to perturbations in chemical and physical oceanography including episodic changes in NADW production hence thermohaline circulation and ice sheet instability (Böhm et al., 2015). During the early glacial-LGM interval at peak sea-ice extension and minimum atmospheric CO_2, a 2-cell ocean circulation model often described for modern and glacial conditions (e.g. Ferrari et al., 2014; Hines et al., 2015; Nadeau et al., 2019; Wilson et al., 2020) requires a highly stratified ocean with mostly isolated lower (deep water) and upper cells. However, this geometry could partially break down during unstable periods of rapid and transient shifts in ocean front positions and the advance/retreat of sea-ice. For example, a temporary breach in lower and upper cell boundaries would promote some connectivity and mixing of otherwise isolated water masses. The widely registered ~25 ka event implicates the rapid incorporation of some deep unventilated NADW-like water and strong diapycnal mixing within the ACC, which formed homogenous circumpolar and intermediate waters with distinctly lower radiocarbon (Hines et al., 2015) and less radiogenic ε_{Nd} (Williams et al., 2021; Piotrowski et al., 2008) fingerprints that spread through the Atlantic-Indian-Pacific sectors of the Southern Ocean.

At the resolution of existing ^{14}C and ε_{Nd} foraminifer and coral records described above, it appears that the behaviours in physical and chemical oceanography differed between the two intervals of sea-ice maxima at ~25 ka and ~20 ka (Fig. 8E). In contrast to 25 ka, the sudden increase in Antarctic sea-ice at the ~20 ka LGM event occurs during relatively greater but fluctuating AMOC strength (Fig. 8C), reduced ACC velocity (Fig. 8C), and a sudden decline in ε_{Nd} LCDW near the Drake Passage that is not registered downstream in the southeast Atlantic and near Kerguelen (Fig. 8A). Although greater sample resolution might resolve similar shifts in water mass interactions across these different sites, the current evidence suggests that the same environmental and hydrographic controls were not operating at these times. To further elucidate the extent and controls on ocean instability throughout this glacial-interglacial period (including LGM-precursor events), higher resolution records from a wider range of sites and archives are needed. Samples from the Southern and Indian oceans are presently limited, mostly due to the lack of well-preserved foraminifers at high latitudes that have historically been the archive of choice for palaeoceanography studies, the logistical difficulties working in such regions, but also the common bias targeting Atlantic and Pacific Ocean sites.

6. Conclusions

This study presents the first ε_{Nd} and radiocarbon records from the southeast Indian Ocean using modern and glacial deep-water corals, which reveal that a dynamic and unstable oceanographic regime pervaded the glacial Southern Ocean. At ~29 ka, Perth Canyon deep UCDW (1788 m) was highly ventilated (~660 B-Atm yrs), whereas its glacial B-Atm ventilation age (~1500–1600 yrs) was similar to present-day seawater at that depth. Conversely, glacial upper UCDW (1558 m) was much younger and similar to SAMW-AAIW (~700 m), suggesting they were essentially homogeneous over this large depth range, which contrasts to their distinctive radiocarbon signatures today. Early indications of the deglaciation is also registered in the Perth Canyon corals from ~19 ka, when the entire UCDW system was becoming significantly more ventilated.

While compositional differences within glacial UCDW imply some depth stratification during the LGM, an apparent breach of the upper and lower ocean cell boundaries of the MOC occurred at 25 ka. This is identified by a concomitant drop then recovery in both ε_{Nd} and $\Delta^{14}C$ glacial SAMW-AAIW in the Perth Canyon, consistent with mid to deep water ε_{Nd} and $\Delta^{14}C$ records from the South Atlantic, Kerguelen, and Tasmania. These significant but short-lived perturbations reflect the injection of poorly ventilated and more Atlantic-like deep water into intermediate depths due to an abrupt mode switch in circumpolar hydrography that propagated across the Southern Ocean.

This study further highlights the benefits offered by deep-water corals, which can provide robust chronologies and reliably constrain temporal changes in different parameters over wide depth ranges within specific water masses. It also demonstrates the potential of such strategically located sites, which can provide invaluable palaeoceanographic information needed to understand the complex ocean interactions and teleconnections across this critically important region.

Author contributions

JT, MM, and PM conceived the study; JT, MM, PM, MT performed fieldwork; JT, PM, JPD, PS, NT-L undertook sample preparation and/or analyses; JT led writing the paper and all authors contributed to and approved the final manuscript.

Declaration of competing interest

The authors declare that they have no known competing financial interests or personal relationships that could have appeared to influence the work reported in this paper.

Acknowledgements

The authors thank the Schmidt Ocean Institute for providing the RV *Falkor* and crew, as well as the deep-sea ROV and pilots from Neptune Marine Services, which enabled us to collect the samples for this study. The Australian Research Council is acknowledged for fellowship funding to JAT (FT160100259) and MM (FL120100049 and CE140100020). Paolo Montagna gratefully acknowledge the support provided by the Italian National Programme of Antarctic Research (PNRA 2013/AZ2.06 Geosmart Project). We also thank Helen Bostock and an anonymous reviewer for their comments that improved the manuscript. This research was conducted in the Perth Canyon Marine Park under permit number AU-COM2014-252, issued by the Director of Parks Australia. The views expressed in this publication do not necessarily represent the views of the Director of Parks Australia or the Australian Government. This is ISMAR-CNR scientific contribution n. 2063.

Appendix A. Supplementary data

Supplementary data to this article can be found online at https://doi.org/10.1016/j.qsa.2022.100052.

References

Adkins, J.F., Boyle, E.A., 1997. Changing atmospheric $\Delta^{14}C$ and the record of deep water paleoventilation ages. Paleoceanography 12, 337–344.

Adkins, J.F., Cheng, H., Boyle, E.A., Druffel, E.R.M., Edwards, R.L., 1998. Deep-sea coral evidence for rapid change in ventilation of the deep North Atlantic 15,400 years ago. Science 280, 725–728.

Amakawa, H., Yu, T.-L., Tazoe, H., Obata, H., Gamo, T., Sano, Y., Shen, C.-C., Suzuki, K., 2019. Neodymium concentration and isotopic composition distributions in the southwestern Indian Ocean and the Indian sector of the Southern Ocean. Chem. Geol. 511, 190–203. https://doi.org/10.1016/j.chemgeo.2019.01.007.

Anderson, R., Ali, S., Bradtmiller, L., Nielsen, S., Fleisher, M., Anderson, B., Burckle, L., 2009. Wind-driven upwelling in the Southern Ocean and the deglacial rise in atmospheric CO2 (New York, N.Y.). Science 323, 1443–1448. https://doi.org/10.1126/science.1167441.

Basak, C., Fröllje, H., Lamy, F., Gersonde, R., Benz, V., Anderson, R.F., Molina-Kescher, M., Pahnke, K., 2018. Breakup of last glacial deep stratification in the South Pacific. Science 359, 900–904.

Bereiter, B., Eggleston, S., Schmitt, J., Nehrbass-Ahles, C., Stocker, T.F., Fischer, H., Kipfstuhl, S., Chappellaz, J., 2015. Antarctic Ice Cores Revised 800KYr CO2 Data. https://www.ncei.noaa.gov/access/paleo-search/study/17975.

Bertram, C.J., Elderfield, H., 1993. The geochemical balance of the rare earth elements and neodymium isotopes in the oceans. Geochem. Cosmochim. Acta. https://doi.org/10.1016/0016-7037(93)90087-D.

Böhm, E., Lippold, J., Gutjahr, M., Frank, M., Blaser, P., Antz, B., Fohlmeister, J., Frank, N., Andersen, M.B., Deininger, M., 2015. Strong and deep Atlantic meridional overturning circulation during the last glacial cycle. Nature 517, 73–76.

Broecker, W.S., Mix, A., Andree, M., Oeschger, H., 1984. Radiocarbon measurements on coexisting benthic and planktic foraminifera shells: potential for reconstructing

ocean ventilation times over the past 20000 years. Nucl. Instrum. Methods Phys. Res., Sect. B 5, 331–339.
Broecker, W.S., Barker, S., Clark, E., Hajdas, I., Bonani, G., Stott, L., 2004. Ventilation of the glacial deep Pacific Ocean. Science 306, 1169–1172.
Burke, A., Robinson, L.F., 2012. The Southern Ocean's role in carbon exchange during the last deglaciation. Science 335, 557–561.
Burton, K.W., Vance, D., 2000. Glacial-interglacial variations in the neodymium isotope composition of seawater in the Bay of Bengal recorded by planktonic foraminifera. Earth Planet Sci. Lett. 176, 425–441.
Champion, D.C., 2013. Neodymium Depleted Mantle Model Age Map of Australia: Explanatory Notes and User Guide. Geoscience Australia, Canberra. https://doi.org/10.11636/Record.2013.044. Record 2013/44.
Copard, K., Colin, C., Douville, E., Freiwald, A., Gudmundsson, G., De Mol, B., Frank, N., 2010. Nd isotopes in deep-sea corals in the North-eastern Atlantic. Quat. Sci. Rev. 29, 2499–2508. https://doi.org/10.1016/j.quascirev.2010.05.025.
De Deckker, P., Moros, M., Perner, K., Jansen, E., 2012. Influence of the tropics and southern westerlies on glacial interhemispheric asymmetry. Nat. Geosci. 5, 266 e269.2012.
De Deckker, P., Moros, M., Perner, K., Blanz, T., Wacker, L., Schneider, R., Barrows, T.T., O'Loingsigh, T., Jansen, E., 2020. Climatic evolution in the Australian region over the last 94 ka - spanning human occupancy - and unveiling the Last Glacial Maximum. Quat. Sci. Rev. 249, 106593 https://doi.org/10.1016/j.quascirev.2020.106593.
DePaolo, D.J., Wasserburg, G.J., 1976. Nd isotopic variations and petrogenetic models. Geophys. Res. Lett. 3, 249–252. https://doi.org/10.1029/GL003i005p00249.
Du, J., Haley, B.A., Mix, A.C., 2020. Evolution of the global overturning circulation since the last glacial maximum based on marine authigenic neodymium isotopes. Quat. Sci. Rev. 241, 106396.
Dubois-Dauphin, Q., Montagna, P., Siani, G., Douville, E., Wienberg, C., Hebbeln, D., Taviani, M., Zhifei, L., Kallel, N., Pons-Branchu, E., Colin, C., 2017. Past hydrological variations of the intermediate water masses of the western Mediterranean Sea during the past 20 ka inferred from neodymium isotopic composition in foraminifera and cold-water corals. Clim. Past 13, 17–37.
Ferrari, R., Jansen, M.F., Adkins, J.F., Burke, A., Stewart, A.L., Thompson, A.F., 2014. Antarctic sea ice control on ocean circulation in present and glacial climates. Proc. Natl. Acad. Sci. U.S.A. 111, 8753–8758.
Fine, R.A., 1993. Circulation of antarctic intermediate water in the south Indian Ocean. Deep Sea Res. 40, 2021–2042.
Frank, M., 2002. Radiogenic isotopes: tracers of past ocean circulation and erosional input. Rev. Geophys. 40, 1001.
Goldstein, S.L., Hemming, S.R., 2003. Long-lived isotopic tracers in oceanography, paleoceanography, and ice-sheet dynamics. In: Treatise on Geochemistry Pergamon, pp. 1–37.
Gottschalk, J., Michel, E., Thole, L.M., Studer, A.S., Hasenfratz, A.P., Schmid, N., Butzin, M., Mazaud, A., Martinez-Garcia, A., Szidat, S., Jaccard, S.L., 2020. Glacial heterogeneity in Southern Ocean carbon storage abated by fast South Indian deglacial carbon release. Nat. Commun. 11, 6192 https://doi.org/10.1038/.
Hines, S.K.V., Southon, J.R., Adkins, J.F., 2015. A high-resolution record of Southern Ocean intermediate water radiocarbon over the past 30,000 years. Earth Planet Sci. Lett. 432, 46–58.
Hogg, A.G., Heaton, T.J., Hua, Q., Palmer, J.G., Turney, C.S.M., Southon, J., Bayliss, A., Blackwell, P.G., Boswijk, G., Bronk Ramsey, C., Pearson, C., Petchey, F., Reimer, P., Reimer, R., Wacker, L., 2020. SHCal20 Southern Hemisphere calibration, 0-55,000 years cal BP. Radiocarbon 62. https://doi.org/10.1017/RDC.2020.59.
Hu, R., Noble, T.L., Piotrowski, A.M., McCave, I.N., Bostock, H.C., Neil, H.L., 2016. Neodymium isotopic evidence for linked changes in Southeast Atlantic and Southwest Pacific circulation over the last 200 kyr. Earth Planet Sci. Lett. 455, 106–114.
Jeandel, C., 1993. Concentration and isotopic composition of Nd in the south Atlantic Ocean. Earth Planet Sci. Lett. 117, 581–591. https://doi.org/10.1016/0012-821X(93)90104-H.
Key, R.M., 2001. Radiocarbon. https://doi.org/10.1006/rwos.2001.0162.
Kohfeld, K.E., Graham, R.M., de Boer, A.M., Sime, L.C., Wolff, E.W., Le Quéré, C., Bopp, L., 2013. Southern Hemisphere westerly wind changes during the Last Glacial Maximum: paleo-data synthesis. Quat. Sci. Rev. 68, 76–95.
Lacan, F., Tachikawa, K., Jeandel, C., 2012. Neodymium isotopic composition of the oceans: a compilation of seawater data. Chem. Geol. 300–301, 177–184. https://doi.org/10.1016/j.chemgeo.2012.01.019.
Lambelet, M., van de Flierdt, T., Butler, E.C.V., Bowie, A.R., Rintoul, S.R., Watson, R.J., Remenyi, T., Lannuzel, D., Warner, M., Robinson, L.F., Bostock, H.C., Bradtmiller, L. I., 2018. The neodymium isotope fingerprint of Adélie coast bottom water, 247–11 Geophys. Res. Lett. 45 (11), 256. https://doi.org/10.1029/2018GL080074.
Laufkötter, C., Vogt, M., Gruber, N., Aumont, O., Bopp, L., Doney, S.C., Dunne, J.P., Hauck, J., John, J., Lima, I.D., 2016. Projected decreases in future marine export production: the role of the carbon flux through the upper ocean ecosystem. Biogeosciences 13, 4023–4047.
López Correa, M., Montagna, P., Joseph, N., Rüggeberg, A., Fietzke, J., Flögel, S., Dorschel, B., Goldstein, S.L., Wheeler, A., Freiwald, A., 2012. Preboreal onset of cold-water coral growth beyond the Arctic Circle revealed by coupled radiocarbon and U-series dating and neodymium isotopes. Quat. Sci. Rev. 34, 24–43.
Mangini, A., Godoy, J.M., Godoy, M.L., Kowsmann, R., Santos, G.M., Ruckelshausen, M., Schroeder-Ritzrau, A., Wacker, L., 2010. Deep sea corals off Brazil verify a poorly ventilated southern Pacific Ocean during H2, H1 and the younger dryas. Earth Planet Sci. Lett. 293, 269–276.
Marcott, S.A., Bauska, T.K., Buizert, C., Steig, E.J., Rosen, J.L., Cuffey, K.M., Fudge, T.J., Severinghaus, J.P., Ahn, J., Kalk, M.L., 2014. Centennial-scale changes in the global carbon cycle during the last deglaciation. Nature 514, 616–619.
Marinov, I., Gnanadesikan, A., Toggweiler, J.R., Sarmiento, J.L., 2006. The southern ocean biogeochemical divide. Nature 441, 964–967.
Matsumoto, K., 2007. Radiocarbon-based circulation age of the world oceans. J. Geophys. Res. 112, C09004. https://doi.org/10.1029/2007JC004095.
McCulloch, M.T., Perfit, M.R., 1981. $^{143}Nd/^{144}Nd$, $^{87}Sr/^{86}Sr$ and trace element constraints on the petrogenesis of Aleutian island arc magmas. Earth Planet Sci. Lett. 56, 167–179.
McCulloch, M., Trotter, J., Falter, J., Pattiaratchi, C., Montagna, P., Taviani, M., Thresher, R., Hosie, A., Garcia-Corral, L., Haig, D., Foglini, F., Agusti, S., Duarte, C., 2017. ROV Exploration of the Perth Canyon and Assessing the Vulnerability of Deep-Sea Corals to Climate Change and Ocean Acidification. Schmidt Ocean Institute Cruise FK150301 Final Report. https://schmidtocean.org/cruise/perth-canyon-first-deep-exploration/.
Meredith, M.P., 2016. Understanding the structure of changes in the Southern Ocean eddy field. Geophys. Res. Lett. 43, 5829–5832.
Moore, J.K., Fu, W., Primeau, F., Britten, G.L., Lindsay, K., Long, M., Doney, S.C., Mahowald, N., Hoffman, F., Randerson, J.T., 2018. Sustained climate warming drives declining marine biological productivity. Science 359, 1139–1143.
Nadeau, L.-P., Ferrari, R., Jansen, M.F., 2019. Antarctic sea ice control on the depth of North Atlantic deep water. J. Clim. 32, 2537–2551.
Orsi, A.H., Johnson, G.C., Bullister, J.L., 1999. Circulation, mixing, and production of antarctic bottom water. Prog. Oceanogr. 43, 55–109. https://doi.org/10.1016/S0079-6611(99)00004-X.
Pahnke, K., Goldstein, S., Hemming, S.R., 2008. Abrupt changes in Antarctic Intermediate Water circulation over the past 25,000 years. Nat. Geosci. 1, 870–874.
Piepgras, J., Wasserburg, J., 1980. Neodymium isotopic variations in seawater. Earth Planet Sci. Lett. 50, 128–138.
Piotrowski, A.M., Goldstein, S.L., Hemming, S.R., Fairbanks, R.G., 2004. Intensification and variability of ocean thermohaline circulation through the last deglaciation. Earth Planet Sci. Lett. 225, 205. https://doi.org/10.1016/j.epsl.2004.06.002 e220.
Piotrowski, A.M., Goldstein, S.L., Hemming, S.R., Fairbanks, R.G., Zylberberg, D.R., 2008. Oscillating glacial northern and southern deep water formation from combined neodymium and carbon isotopes. Earth Planet Sci. Lett. 272, 394–405.
Piotrowski, A.M., Banakar, V.K., Scrivner, A.E., Elderfield, H., Galy, A., Dennis, A., 2009. Indian Ocean circulation and productivity during the last glacial cycle. Earth Planet Sci. Lett. 285, 179–189. https://doi.org/10.1016/j.epsl.2009.06.007.
Pöppelmeier, F., Lippold, J., Blaser, P., Gutjahr, M., Frank, M., Stocker, T.F., 2022. Neodymium isotopes as a paleo-water mass tracer: a model-data reassessment. Quat. Sci. Rev. 279, 107404.
Rennie, S., Hanson, C.E., McCauley, R.D., Pattiaratchi, C., Burton, C., Bannister, J., Jenner, C., Jenner, M.-N., 2009. Physical properties and processes in the Perth Canyon, Western Australia: links to water column production and seasonal pygmy blue whale abundance. J. Mar. Syst. 77, 21–44. https://doi.org/10.1016/j.jmarsys.2008.11.008.
Rintoul, S.R., 2007. Rapid freshening of antarctic bottom water formed in the Indian and Pacific oceans. Geophys. Res. Lett. 34, L06606. https://doi.org/10.1029/2006GL028550.
Rintoul, S.R., 2018. The global influence of localized dynamics in the Southern Ocean. Nature 558, 209–218.
Rintoul, S.R., Naveira Garabato, A.C., 2013. Dynamics of the Southern Ocean circulation. Ocean Circ. Clim. 103 https://doi.org/10.1016/B978-0-12-391851-2.00018-0.
Rintoul, S.R., Chown, S.L., DeConto, R.M., England, M.H., Fricker, H.A., Masson-Delmotte, V., Naish, T.R., Siegert, M.J., Xavier, J.C., 2018. Choosing the future of Antarctica. Nature 558, 233–241.
Robinson, L.F., van de Flierdt, T., 2009. Southern Ocean evidence for reduced export of North Atlantic deep water during Heinrich event 1. Geology 37, 195–198.
Robinson, L.F., Adkins, J.F., Keigwin, L.D., Southon, J., Fernandez, D.P., Wang, S.L., Scheirer, D.S., 2005. Radiocarbon variability in the western North Atlantic during the last deglaciation. Science 310, 1469–1473.
Robinson, L.F., Adkins, J.F., Frank, N., Gagnon, A.C., Prouty, N.G., Brendan Roark, E., van de Flierdt, T., 2014. The geochemistry of deep-sea coral skeletons: a review of vital effects and applications for palaeoceanography. Deep Sea Res. Part II Top. Stud. Oceanogr. 99, 184–198.
Ronge, T.A., Prange, M., Mollenhauer, G., Ellinghausen, M., Kuhn, G., Tiedemann, R., 2020. Radiocarbon evidence for the contribution of the Southern Indian Ocean to the evolution of atmospheric CO2 over the last 32,000 years. Paleoceanogr. Paleoclimatol. 35 https://doi.org/10.1029/2019PA003733 e2019PA003733.
Sarmiento, J., Gruber, N., Brzezinski, M., Dunne, J., 2004. High-latitude controls of thermocline nutrients and low latitude biological productivity. Nature 4276969, 56–60.
Schulz, K.G., Zeebe, R.E., 2006. Pleistocene glacial terminations triggered by synchronous changes in Southern and Northern Hemisphere insolation: the insolation canon hypothesis. Earth Planet Sci. Lett. 249, 326–336. https://doi.org/10.1016/j.epsl.2006.07.004.
Sigman, D.M., Hain, M.P., Haug, G.H., 2010. The polar ocean and glacial cycles in atmospheric CO2 concentration. Nature 466, 47–55.
Skinner, L., Fallon, S., Waelbroeck, C., Michel, E., Barker, S., 2010. Ventilation of the deep Southern Ocean and deglacial CO2 rise. Science 328, 1147–1151.
Skinner, L.C., Scrivner, A.E., Vance, D., Barker, S., Fallon, S., Waelbroeck, C., 2013. North Atlantic versus Southern Ocean contributions to a deglacial surge in deep ocean ventilation. Geology 41, 667–670.

Struve, T., Wilson, D.J., van de Flierdt, T., Pratt, N., Crocket, K.C., 2020. Middle Holocene expansion of Pacific deep water into the Southern Ocean. Proc. Natl. Acad. Sci. U.S.A. 117, 889–894.

Tachikawa, K., Arsouze, T., Bayon, G., Bory, A., Colin, C., Dutay, J.-C., Frank, N., Giraud, X., Gourlan, A.T., Jeandel, C., Lacan, F., Meynadier, L., Montagna, P., Piotrowski, A.M., Plancherel, Y., Pucéat, E., Roy-Barman, M., Waelbroeck, C., 2017. The large-scale evolution of neodymium isotopic composition in the global modern and Holocene ocean revealed from seawater and archive data. Chem. Geol. https://doi.org/10.1016/j.chemgeo.2017.03.018.

Toggweiler, J.R., Russell, J., 2008. Ocean circulation in a warming climate. Nature 451, 286.

Toggweiler, J.R., Russell, J.L., Carson, S.R., 2006. Midlatitude westerlies, atmospheric CO_2, and climate change during the ice ages. Paleoceanography 21, PA2005. https://doi.org/10.1029/2005PA001154.

Trotter, J.A., Pattiaratchi, C., Montagna, P., Taviani, M., Falter, J., Thresher, R., Hosie, A., Haig, D., Foglini, F., Hua, Q., McCulloch, M.T., 2019. First ROV exploration of the Perth Canyon: canyon setting, faunal observations, and anthropogenic impacts. Front. Mar. Sci. 6 (173), 1–24. https://doi.org/10.3389/fmars.2019.00173.

van de Flierdt, T., Robinson, L.F., Adkins, J.F., 2010. Deep-sea coral aragonite as a recorder for the neodymium isotopic composition of seawater. Geochem. Cosmochim. Acta 74, 6014–6032.

van de Flierdt, T., Griffiths, A.M., Lambelet, M., Little, S.H., Stichel, T., Wilson, D.J., 2016. Neodymium in the oceans: a global database, a regional comparison and implications for palaeoceanographic research. Philos. Trans. R. Soc., Math. Phys. Eng. Sci. 374 https://doi.org/10.1098/rsta.2015.0293.

van Wijk, E.M., Rintoul, S.R., Ronai, B.M., Williams, G.D., 2010. Regional circulation around Heard and McDonald Islands and through the fawn trough, central Kerguelen Plateau. Deep Sea Res. Oceanogr. Res. Pap. 57, 653–669.

WAIS 2013 Divide Project Members, 2013. Onset of deglacial warming in West Antarctica driven by local orbital forcing. Nature 500, 440–444.

WAIS Divide Project Members, 2015. Precise interpolar phasing of abrupt climate change during the last ice age. Nature 520, 661–665.

Williams, T.J., Martin, E.E., Sikes, E., Starr, A., Umling, N.E., Glaubke, R., 2021. Neodymium isotope evidence for coupled Southern Ocean circulation and Antarctic climate throughout the last 118,000 years. Quat. Sci. Rev. 260 https://doi.org/10.1016/j.quascirev.2021.106915.

Wilson, D.J., Piotrowski, A.M., Galy, A., McCave, I.N., 2012. A boundary exchange influence on deglacial neodymium isotope records from the deep western Indian Ocean, 0 Earth Planet Sci. Lett. 341–344, 35–47.

Wilson, D.J., Crocket, K.C., van de Flierdt, T., Robinson, L.F., Adkins, J.F., 2014. Dynamic intermediate ocean circulation in the North Atlantic during Heinrich Stadial 1: a radiocarbon and neodymium isotope perspective. Paleoceanography 29, 1072–1093. https://doi.org/10.1002/2014PA002674.

Wilson, D.J., Piotrowski, A.M., Galy, A., Banakar, V.K., 2015. Interhemispheric controls on deep ocean circulation and carbon chemistry during the last two glacial cycles. Paleoceanography 30, 621–641. https://doi.org/10.1002/2014PA002707.

Wilson, D.J., Struve, T., van de Flierdt, T., Chen, T., Li, T., Burke, A., Robinson, L.F., 2020. Sea-ice control on deglacial lower cell circulation changes recorded by Drake Passage deep-sea corals. Earth Planet Sci. Lett. 544 https://doi.org/10.1016/j.epsl.2020.116405.

Wong, A.P.S., 2005. Subantarctic mode water and Antarctic intermediate water in the south Indian Ocean based on profiling float data 2000–2004. J. Mar. Res. 63, 789–812. https://doi.org/10.1357/0022240054663196.

Woo, M., Pattiaratchi, C., 2008. Hydrography and water masses off the Western Australian coast. Deep-Sea Res. I 55, 1090–1104. https://doi.org/10.1016/j.dsr.2008.05.005.

Wu, S., Lembke-Jene, L., Lamy, F., Arz, H.W., Nowaczyk, N., Xiao, W., Zhang, X., Hass, H.C., Titschack, J., Zheng, X., Liu, J., Dumm, L., Diekmann, B., Nürnberg, D., Tiedemann, R., Kuhn, G., 2021. Orbital- and millennial-scale Antarctic Circumpolar Current variability in Drake Passage over the past 140,000 years. Nat. Commun. https://doi.org/10.1038/s41467-021-24264-9.

Xiao, W., Esper, O., Gersonde, R., 2016. Last glacial—holocene climate variability in the Atlantic sector of the Southern Ocean. Quat. Sci. Rev. 135, 115–137. https://doi.org/10.1016/j.quascirev.2016.01.023.

Yu, Z., Colin, C., Ma, R., Meynadier, L., Wan, S., Wu, Q., Kallel, N., Sepulcre, S., Dapoigny, A., Bassinot, F., 2018. Antarctic intermediate water penetration into the northern Indian Ocean during the last deglaciation. Earth Planet Sci. Lett. 500, 67–75. https://doi.org/10.1016/j.epsl.2018.08.006.

Zhao, N., Oppo, D.W., Huang, K.-F., Howe, J.N.W., Blusztajn, J., Keigwin, L.D., 2019. Glacial–interglacial Nd isotope variability of North Atlantic Deep Water modulated by North American ice sheet. Nat. Commun. https://doi.org/10.1038/s41467-019-13707-z.